Electronic Supplementary Material (ESI) for Journal of Materials Chemistry A.

2D-on-2D core-shell $Co_3(PO_4)_2$ stacked micropetals@$Co_2Mo_3O_8$ nanosheets and binder-free 2D CNT-$Ti_3C_2T_X$–MXene electrodes for high-energy solid-state flexible supercapacitor

Amar. M. Patil[a], Nilesh. R. Chodankar[b], Euigeol. Jung[a], Sanjib. Roy[a], Deepak. P. Dubal[c], Guoqing Guan[d], Young-Kyu Han[b], Seong Chan Jun[a]*

[a]Nano-Electro-Mechanical Device Laboratory School of Mechanical Engineering, Yonsei University Seoul 120-749, South Korea

[b]Department of Energy and Material Engineering, Dongguk University-Seoul, Seoul 04620, South Korea

[c]Centre for Materials Science, School of Chemistry and Physics, Queensland University of Technology (QUT), 2 George Street, Brisbane 4000, Australia

[d]Energy Conversion Engineering Laboratory, Institute of Regional Innovation (IRI), Hirosaki University, 2-1-3 Matsubara, Aomori 030-0813, Japan

*Corresponding Author
Prof. Seong Chan Jun
E-mail: scj@yonsei.ac.kr

1. Experimental Section

1.1 Chemicals - Layered ternary carbide Ti_3AlC_2 (MAX phase) (particle size < 40 μm), ammonium phosphate monobasic ($(NH_4)H_2PO_4$, 98%), urea (CH_4N_2O, 99 –100.5%), poly(vinyl alcohol) ($(C_2H_4O)x$, Mw 85,000–124000, 99 %) and potassium hydroxide (KOH, ≥85 %) purchased from Sigma-Aldrich. Hydrochloric acid (HCl, 37 %), lithium fluoride (LiF, 98.5 %) and disodium molybdate (VI) dihydrate ($Na_2MoO_4.2H_2O$, 98.5 %) were purchased from Across Organics, Alfa Aesar and Junsei chemicals, respectively. Cobalt nitrate hexahydrate ($Co(NO_3)_2.6H_2O$. 97%), nitric acid (HNO_3, 68-70 %) and ethanol (C_2H_5OH, 95 %) purchased from SAMCHUN chemicals. Carbon cloth (CC) purchased from NARA Cell-Tech Corporation with model of W0S1009 (W0S1002) and carbon nanotubes (CNT) (diameter of ≈ 23 nm).

1.2 Synthesis of $Co_3(PO_4)_2$@$Co_2Mo_3O_8$ 2D-on-2D core-shell TSM@NS electrodes

All purchased chemicals were used as it is without further purification process. Synthesis process of the electrode was carried out in two step processes; first step was the hydrothermal synthesis of 2D self-assembled transparent stacked micropetals (TSM) of $Co_3(PO_4)_2$, and second step was chronoamperometric electrodeposition of nanosheets (NS) of $Co_2Mo_3O_8$. Prior to deposition, the CC substrates were cleaned with concentrated HNO_3 and subsequently washed, ultrasonicated with deionized water and ethanol for 20 min and dried in the vacuum oven for overnight. Hydrothermal method was used to make 2D TSM of $Co_3(PO_4)_2$ on the CC, with $Co(NO_3)_2.6H_2O$ as a cobalt source and $NH_4H_2PO_4$ as a phosphate source. In typical synthesis, the 0.05 $Co(NO_3)_2.6H_2O$, 0.1 M $NH_4H_2PO_4$ and 0.5 M CH_4N_2O were then dissolved in the 50 ml DI water and stirred for 10 minutes. In the next step, the prepared solution was transferred to a Teflon-lined stainless-steel autoclave and the cleaned CC substrate (3 × 4 cm^2) was immersed in it. The autoclave was heated at 180 ºC for 12 h and then allowed to cool down naturally at room temperature (~25 ºC). $Co_3(PO_4)_2$ on CC 2D TSM was

synthesized and dried at 60°C for 6 hours before being annealed at 400 °C for 5 hours. For the better comparative study of the electrochemical output of the electrodes, the electrode was optimized by taking deposition at additional two different temperatures of 160 ºC and 200 ºC while maintaining same deposition time. In the second step, the Co-Mo-precursor NS was electrodeposited on the best performance $Co(NO_3)_2$/CC 2D TSM electrode at different concentrations of the Co-Mo precursors. The 50 ml electrolyte solution was prepared by addition of $Co(NO_3)_2.6H_2O$, and Na_2MoO_4 reagents in the molar percentage ratio of 1:2, 1:1 and 2:1, respectively. Furthermore, the 0.05 M urea was added in the above solutions. In the three electrode system, platinum wire, Hg/HgO, and deposited electrodes (2 × 2 cm^2) were used as the counter, reference, and working electrodes, respectively. The chronoamperometric electrodeposition was performed at constant potential of –1.1 V. However, the uniform deposition condition was achieved by varying the time of deposition from 300 – 900 seconds. Uniform and high-performance electrodes were deposited at a deposition time of 600 seconds. After electrodeposition, the electrodes were rinsed in the DI water and then dried in vacuum oven at 60 ºC for 6 hours, followed by annealing at 530 ºC for 2 h in the protection of Ar/H_2 atmosphere. Synthesized electrodes before annealing at 530 ºC at different Co-Mo precursors molar concentrations of 1:2, 1:1 and 2:1 was abbreviated as CoPO-CMO12, CoPO-CMO11 and CoPO-CMO21. Further, CoPO-CMO21 electrode was abbreviated as CoPO-CMO238 after being annealed at 530 ^{0}C for 2 hours in an Ar/H_2 atmosphere. The mass loading on the electrodes was measured using a sensitive microbalance (Model PAG214, OHAUS). The mass loading of one side deposited active electrode materials on the CC surface ranged from 0.5 to 0.8 mg cm^{-2}.

1.3 Synthesis of 2D CNT-$Ti_3C_2T_X$/CC electrodes

Initially, the 0.5 g of carbon nanotubes were added in 20 ml concentrated HNO_3 and ultrasonicated for 5 h. The activated CNTs were then washed several times with DI water to

neutralize the pH. The washed CNTs were then dried for 24 hours in a vacuum oven at 60 °C. $Ti_3C_2T_X$-MXene were synthesized by *in-situ* HF etching of Ti_3AlC_2-MAX phase. The etched product was exfoliated and delaminated using the minimal intensive layered delamination (MILD) method. In typical synthesis, the 0.8 g of LiF and 0.5 g Ti_3AlC_2 powder were slowly added in the 15 ml 9 M HCl solution and stirred continuously at 35 ºC for 24 hours. Following the etching process, the product was washed several times in DI water and centrifuged for 5 minutes at 3500 rpm using centrifuge machine (LABOGENE 1248). The ink-like supernatant of $Ti_3C_2T_X$ was collected after the pH of the etched solution reached up to 6 to 7. Furthermore, the 20 ml of $Ti_3C_2T_X$ ink solution and 0.02 g of activated CNTs was added and ultrasonicated for 1 hour and then this homogeneous ink-like solution dropped onto surface of CC substrate and dried at 50 ºC for 2 hours in vacuum oven. To obtain the appropriate thickness and mass loading of electroactive material, the drop casting and drying procedure was repeated several times. The electrode mass loading of 0.8~1.0 mg cm^{-2} was adjusted for CNT-$Ti_3C_2T_X$/CC electrode.

1.4 Characterization of materials

A Rigaku diffractometer (Maxima XRD-7000) with Cu K alpha radiation (λ= 1.5406 A.U.) was used to study the structural properties of the electrodes. The surface morphology of the electrodes was studied using Model MIRA3 TESCAN scanning electron microscopy (SEM) and field emission SEM (FESEM), JEOL-7800F. Model K-alpha (Thermo Scientific Inc., U.K) with X-ray source of Al Ka μ-focused monochromator (1486.6 eV) and X-ray power of 12 kV, 3 mA, was employed to analyze the chemical composition and the oxidation characteristics of the electrode materials. Transmission electron microscopy (TEM), Model JEOL JEM-2010 was employed to analyze surface morphology and elemental mapping of the material. Model Autosorb-iQ 2ST/MP Quantachrome was used to analyze surface area and pore size distribution. The temperature of the FHSCs device was accurately measured using

thermal camera (FLIR). The electrode as well as supercapacitor device electrochemical parameters were measured using the electrochemical workstation ZIVE SP2. The regulated DC power supply (LPS-305TP) was used to charge the supercapacitor devices at constant voltage during demonstration of FHSCs.

1.5 Electrochemical measurements

The electrochemical measurements of the all electrodes as well as solid-state supercapacitor device were carried out in three-as well as two electrode system. In three electrode system, platinum wire, Hg/HgO and prepared electrodes were used as counter, reference and working electrodes, respectively. CV, GCD and EIS electrochemical measurements of the electrodes in the three-electrode system were carried out in the 3 M KOH electrolyte. The cycling stability of the electrodes as well as supercapacitor devices were estimated by repeating the GCD cycles.

1.6 Fabrication of flexible hybrid solid-state supercapacitor (FHSCs) device

FHSCs was fabricated by employing core-shell structured CoPO-CMO238 2D-on-2D TSM@NS positive electrode and 2D CNTs-$Ti_3C_2T_X$/CC composites negative electrode with polyvinyl alcohol-potassium hydroxide (PVA-KOH) electrolyte (acts as electrolyte as well as separator). PVA-KOH gel electrolyte was prepared by dissolving 3 g of PVA in 30 ml DI water at 70 ºC with continuous stirring followed by addition of 3 M KOH. The prepared electrolyte was transparent and used as it is as electrolyte and separator to assemble FHSCs devices. The charge balancing of the positive and negative electrodes were carried out to achieve the higher electrochemical performance. The charge balancing was attained by adjusting the mass ratios of the electrodes by using following equation.

$$\frac{m_+}{m_-} = \frac{C_- V_-}{C_+ V_+} \quad (1)$$

Where, m^+, m^- and C^+, C^- are masses and specific capacitances of the positive and negative electrodes for 1 cm^2 area, respectively. The mass ratios of the positive to negative electrode was maintained as 1:4.4.

The specific capacity (Q_s), specific, areal and volumetric capacitances (C_s, C_A and C_V) of the electrodes were calculated using following equations.

$$Specific\ capacity\ (Qs) = \frac{I\ \times\ \Delta t}{m\ \times\ 3.6} \quad (2)$$

$$Specific\ capacitance\ (C_s) = \frac{I\ \times\ \Delta t}{m\ \times\ \Delta V} \quad (3)$$

$$Areal\ capacitance\ (C_A)\ = \frac{I\ \times\ \Delta t}{Area\ \times\ \Delta V} \quad (4)$$

$$Volumetric\ capacitance\ (C_V) = \frac{I\ \times\ \Delta t}{Volume\ \times\ \Delta V} \quad (5)$$

Where, I is applied current, Δt is discharge time, $^{\Delta}V$ is operating potential window, C_S, C_A, C_V are specific, areal, and volumetric capacitances.

The specific, areal and volumetric energy as well as power of FHSCs device were calculated by applying below equations.

$$E_S = (C_S \times \Delta V^2)/(2 \times 3600) \quad (6)$$

$$E_A = (C_A \times \Delta V^2)/(2 \times 3600) \quad (7)$$

$$E_V = (C_V \times \Delta V^2)/(2 \times 3600) \quad (8)$$

$$P = (3600 \times E)/\Delta t \quad (9)$$

Similarly, specific, areal as well as volumetric power, P (W kg^{-1}, W cm^{-2} and W cm^{-3}) of FHSCs device were calculated using Equation S8. Furthermore, the energy efficiencies of the FHSCs device were calculated using following equation.

$$\text{Energy efficiency} = E_{discharge} \times 100/E_{charge} \quad (10)$$

Electrochemical reactions on $Co_3(PO_4)_2$@$Co_2Mo_3O_8$ positive electrode

$$Co_3(PO_4)_2 + OH^- \leftrightarrow Co_3(PO_4)_2(OH) + e^- \quad (11)$$

$$Co_2Mo_3O_8 + 2OH^- \rightarrow 2CoOOH + 3MoO_2 + e^- \quad (12)$$

$$CoOOH + OH^- \leftrightarrow CoO_2 + H_2O + e^- \quad (13)$$

$$CoOOH + H_2O + e^- \leftrightarrow Co(OH)_2 + OH^- \quad (14)$$

Electrochemical reactions on CNT-$Ti_3C_2T_X$ positive electrode

$$Ti_3C_2T_x + xK^+ + xe^- \leftrightarrow K_xTi_3C_2T_x \quad (15)$$

$$Ti_3C_2 + xK^+ + xe^- \leftrightarrow K_xTi_3C_2 \quad (16)$$

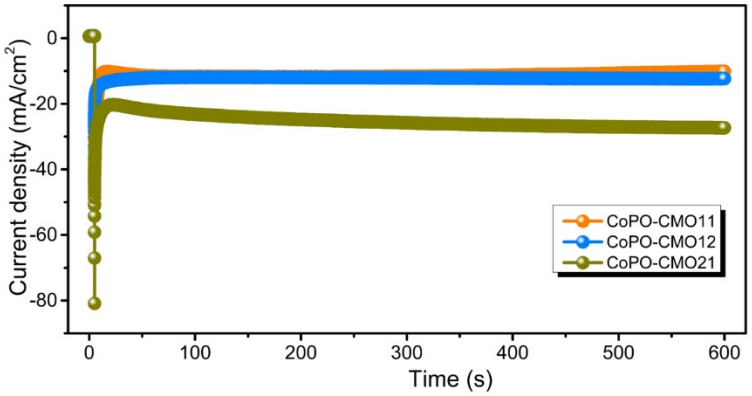

Figure S1 Chronoamperometry plots of current density versus time for CoPO-CMO11, CoPO-CMO12 and CoPO-CMO21 samples.

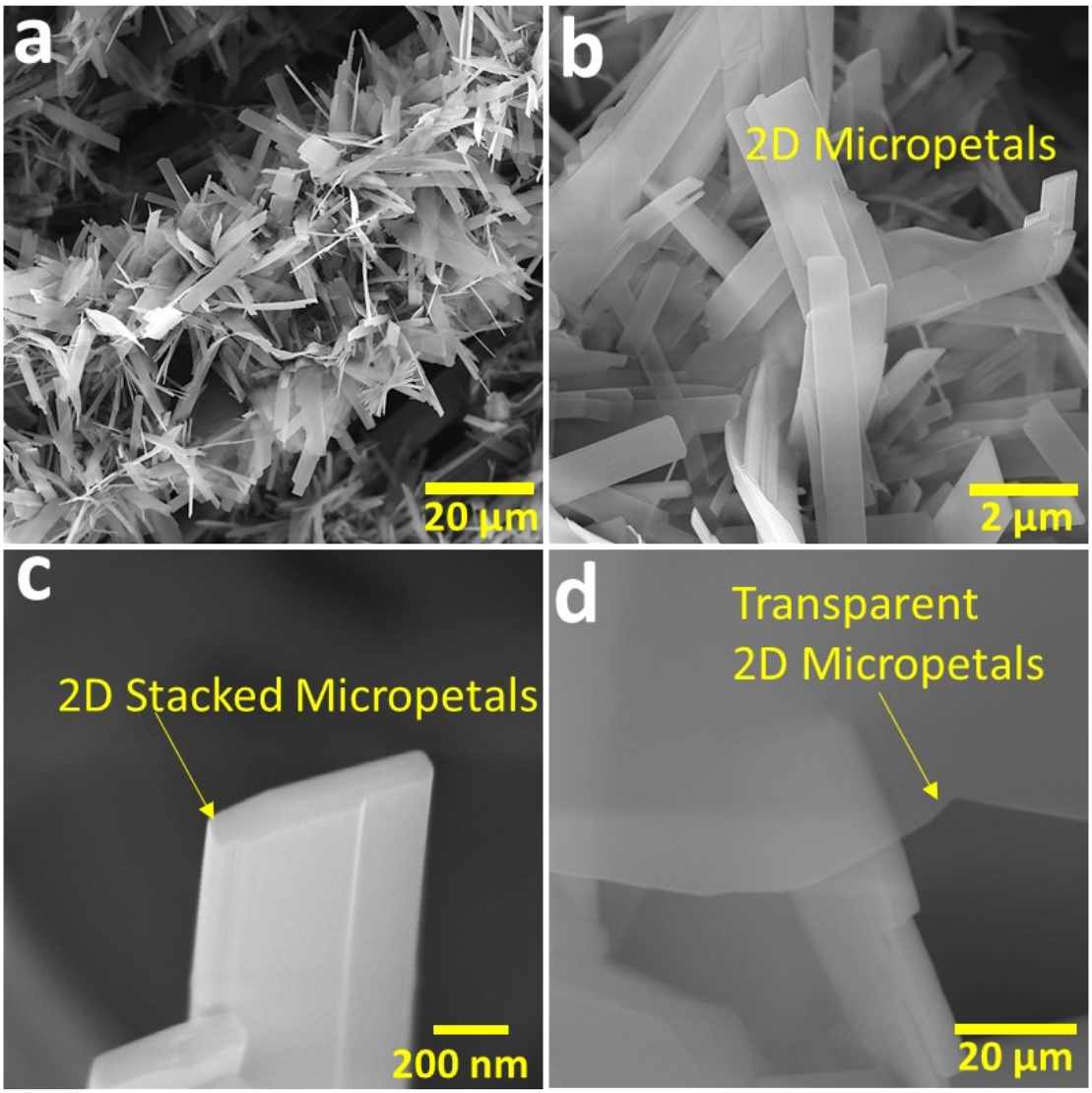

Figure S2 (a-d) SEM images of the $Co_3(PO_4)_2$/CC electrodes, showing stacked as well as exfoliated 2D TSM on CC.

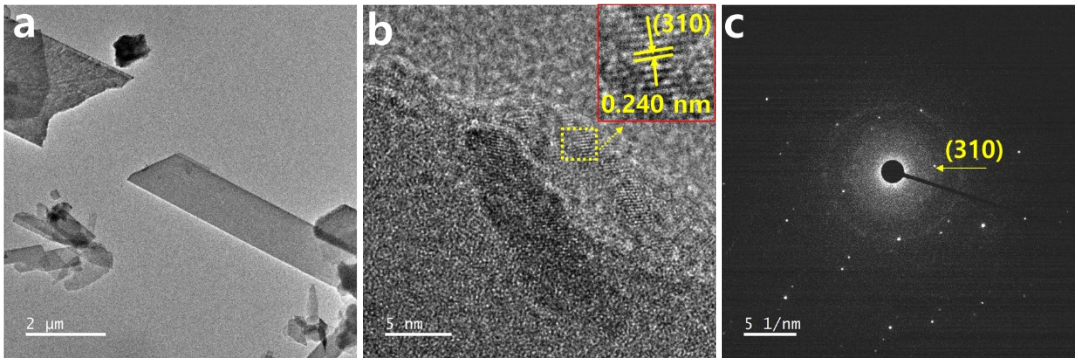

Figure S3 (a and b) TEM and HRTEM images and (c) SAED pattern of the $Co_3(PO_4)_2$ TSM.

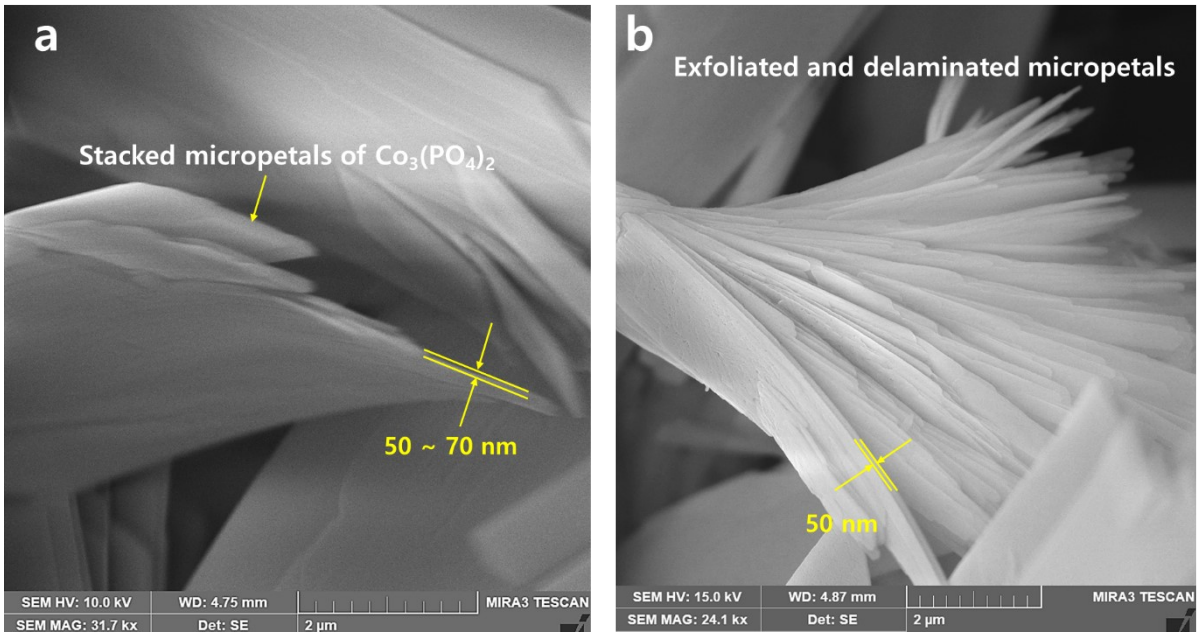

Fig. S4 (a and b) SEM images of the $Co_3(PO_4)_2$ stacked micropetals.

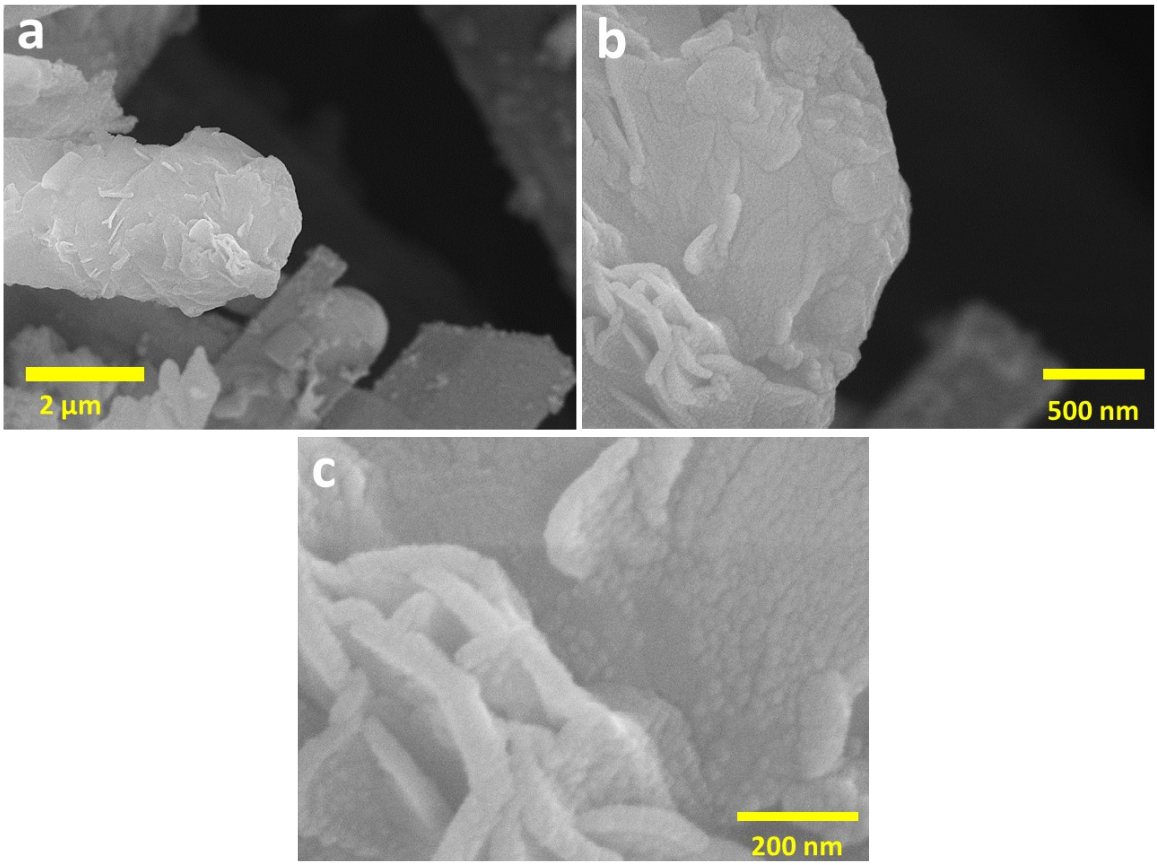

Figure S5 (a-c) SEM images of the sample CoPO-CMO12 at different magnifications showing thick layer of Co-Mo-precursor nanosheets on the $Co_3(PO_4)_2$ 2D TSM.

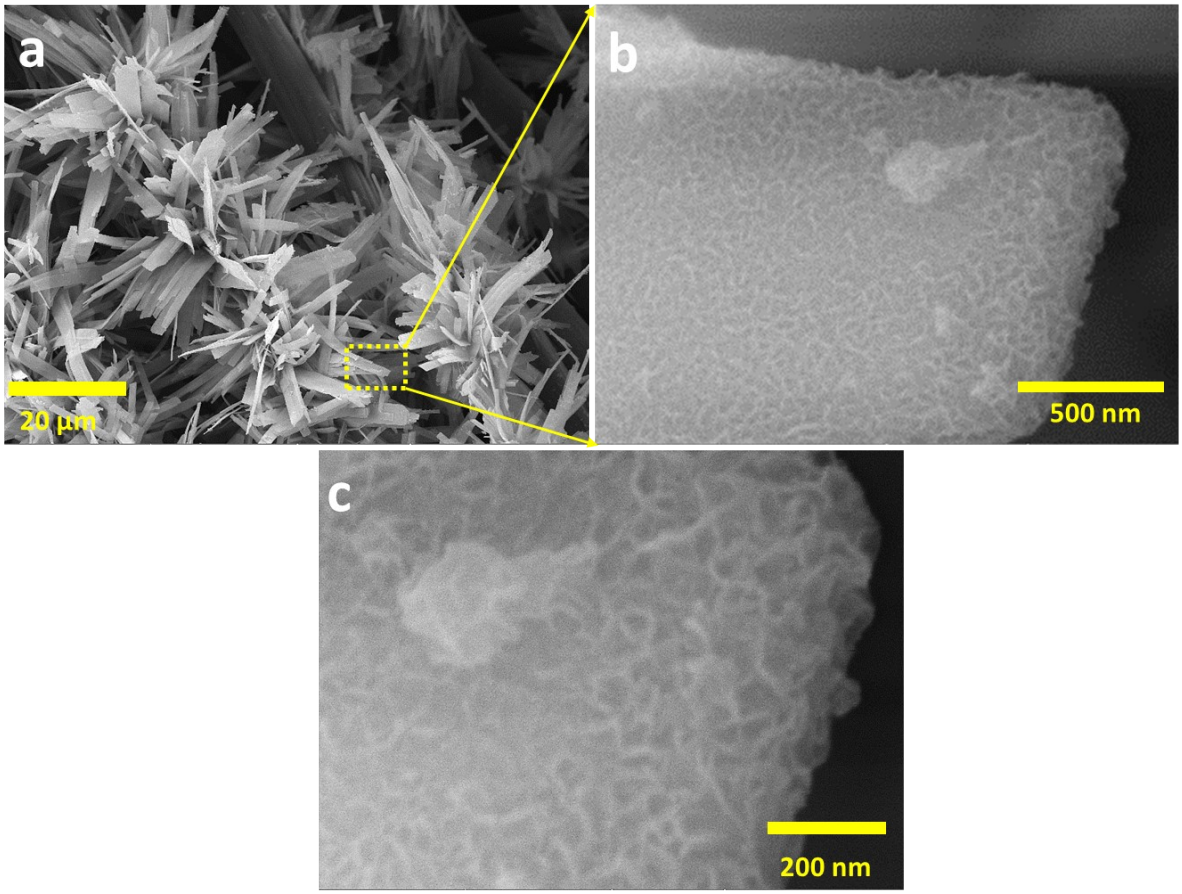

Figure S6 (a-c) SEM images of the sample CoPO-CMO11 at different magnifications showing thin layer of interconnected nanosheets on the $Co_3(PO_4)_2$ 2D TSM.

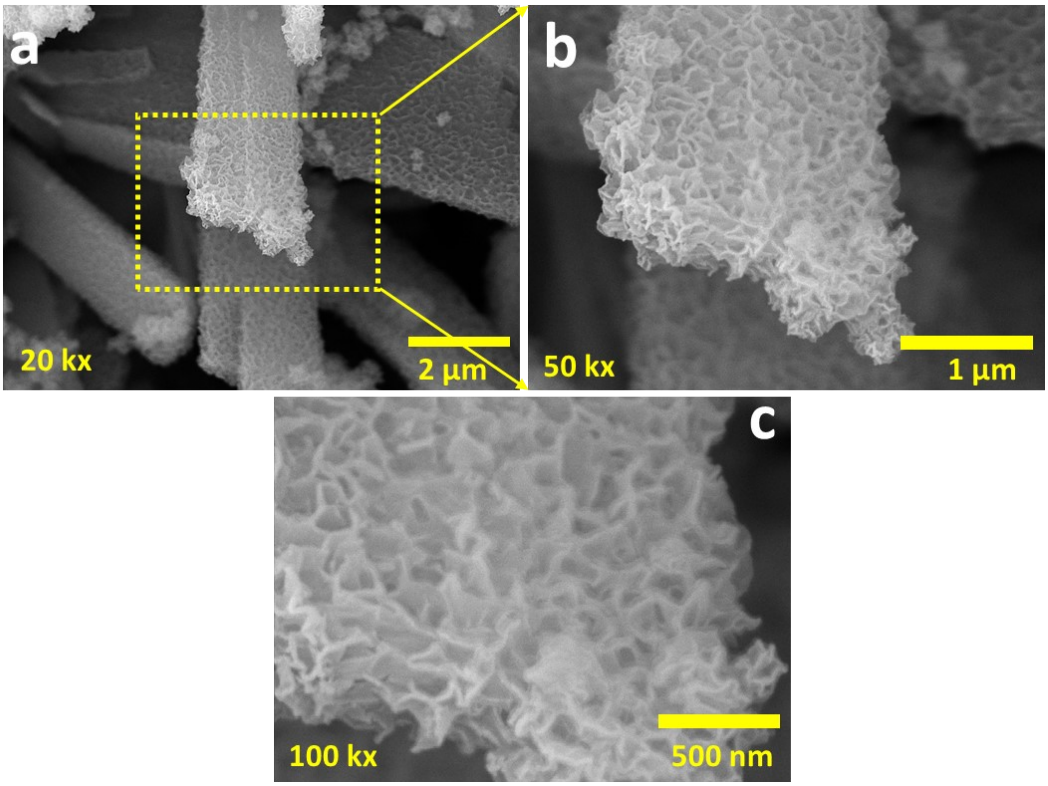

Figure S7 (a-c) SEM images of the CoPO-CMO21 electrode at different magnifications showing uniform thin layer of nanostructure on the $Co_3(PO_4)_2$ 2D TSM.

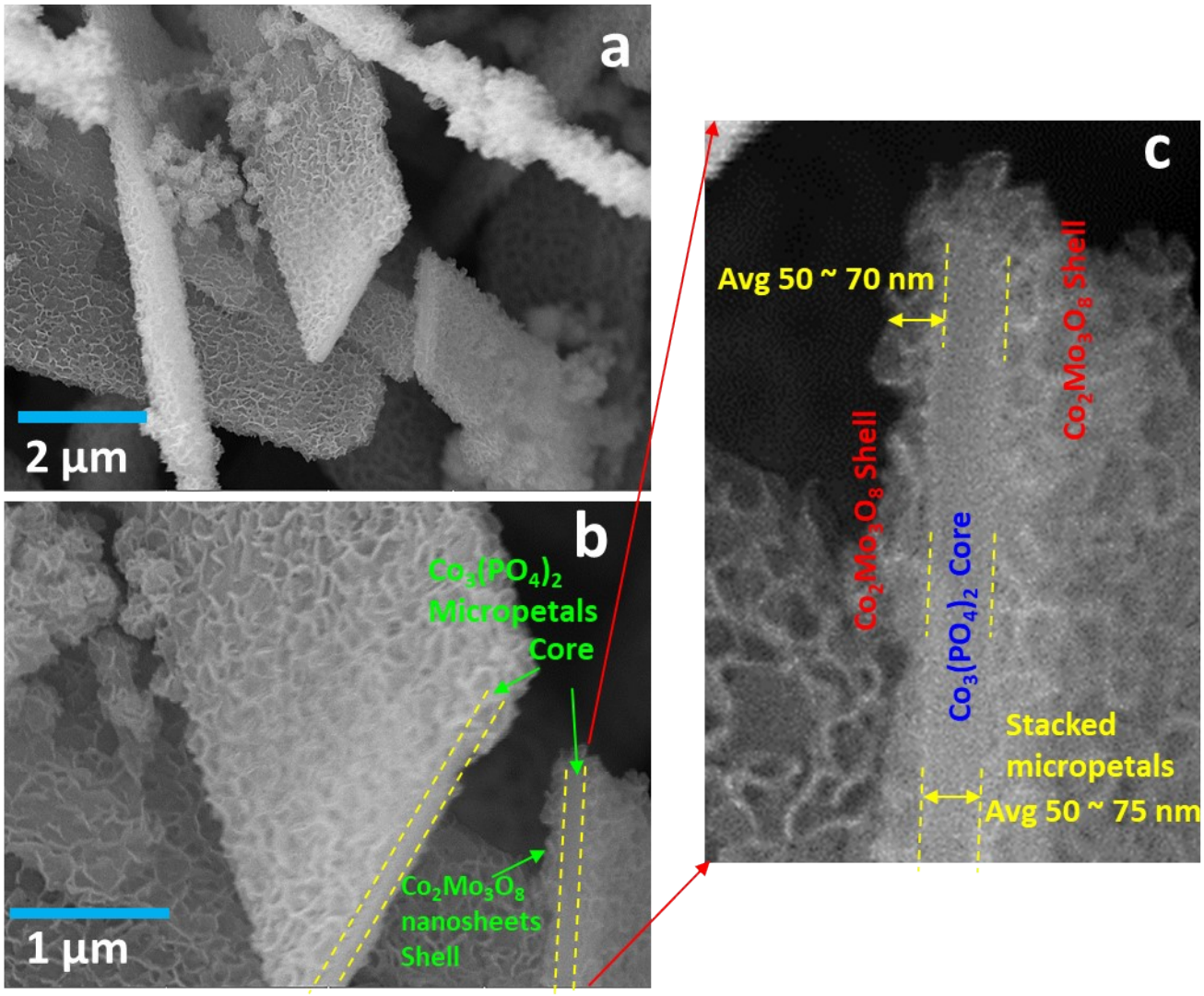

Figure S8 (a-c) SEM images of the CoPO-CMO238 electrode at different magnifications showing uniform thin layer of nanostructure on the $Co_3(PO_4)_2$ core and $Co_2Mo_3O_8$ shell.

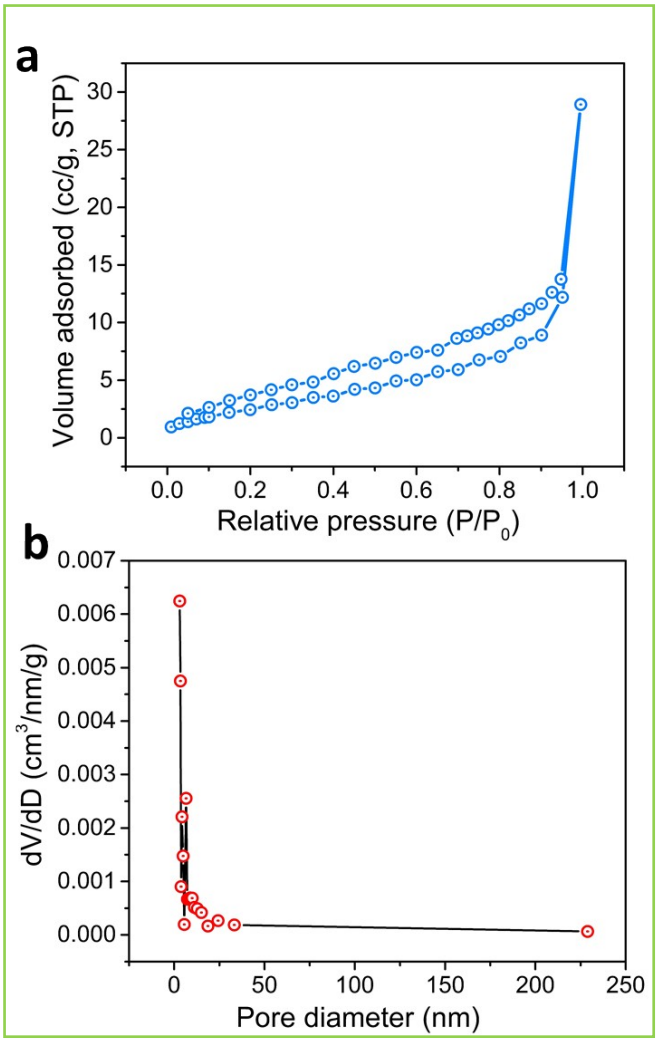

Figure S9 (a) Nitrogen adsorption-desorption isotherms and (b) BJH pore size distribution plots of CoPO-CMO238 2D-on-2D TSM@NS electrode.

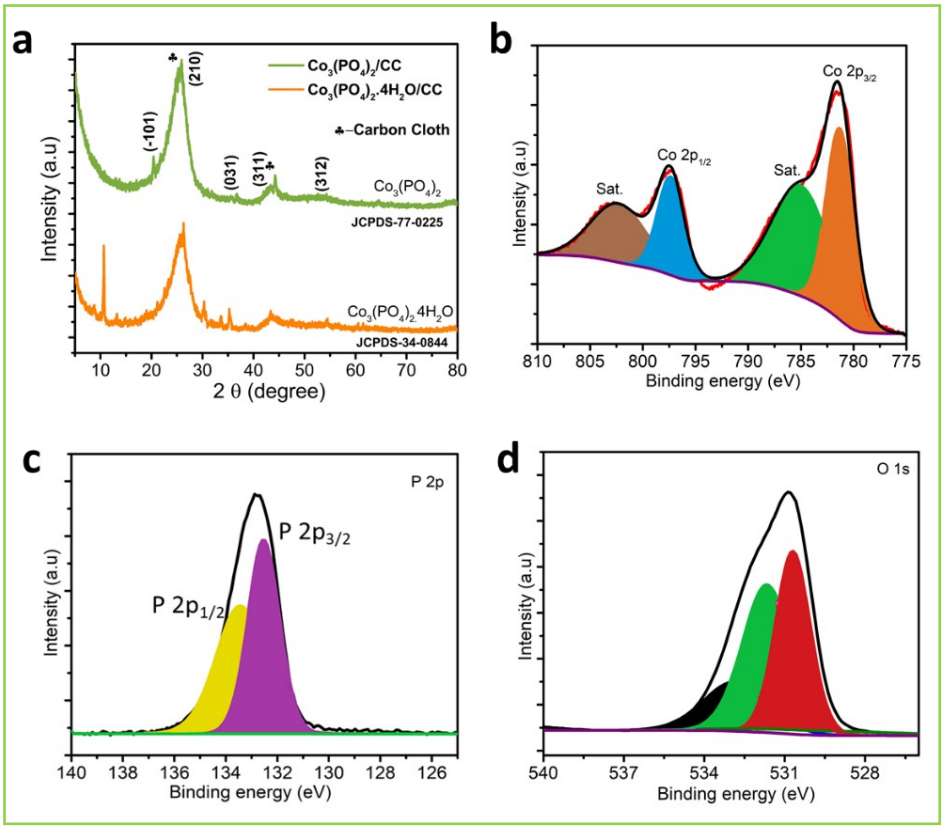

Figure S10 (a) XRD pattern of the $Co_3(PO_4)_2$/CC and $Co_3(PO_4)_2$@$Co_2Mo_3O_8$/CC electrodes, and XPS narrow scan spectra of $Co_3(PO_4)_2$ electrode material for (b) Co 2p, (c) P 2p, and (d) O 1s, respectively.

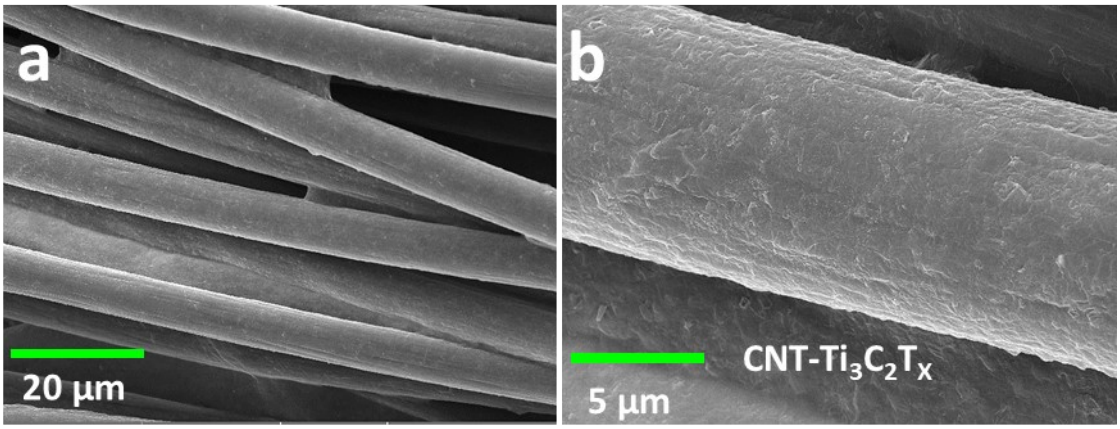

Figure S11 (a and b) SEM images of the CNT-$Ti_3C_2T_X$/CC electrode at different magnifications.

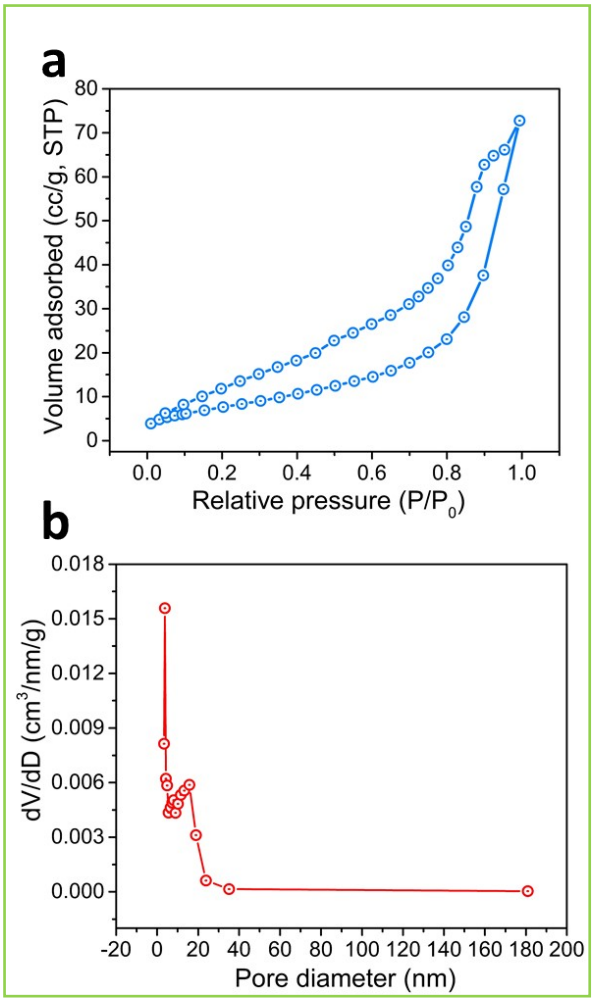

Figure S12 (a) Nitrogen adsorption-desorption isotherms and (b) BJH pore size distribution plots of CNT-$Ti_3C_2T_X$ electrode material.

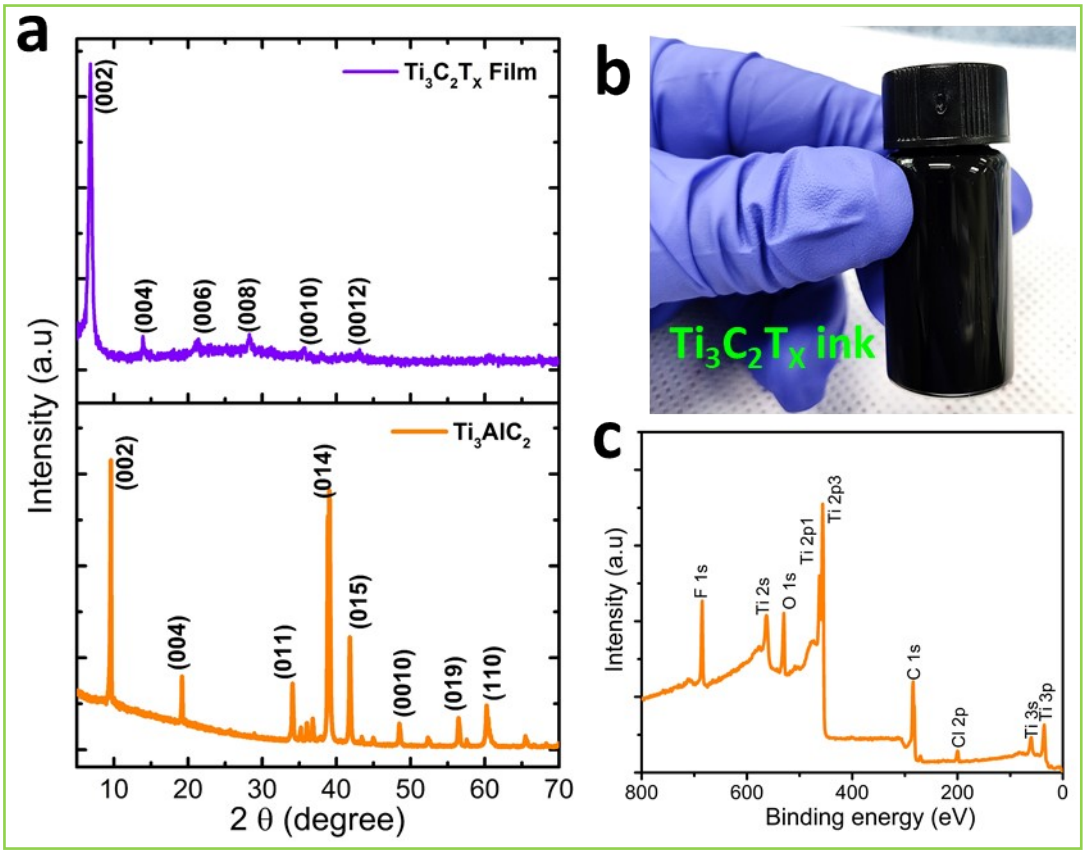

Figure S13 (a) XRD patterns of the Ti_3AlC_2 (MAX phase) and $Ti_3C_2T_X$ (MXene), (b) synthesized delaminated MXene solution, and (c) XPS survey spectrum of CNT-$Ti_3C_2T_X$/CC electrode.

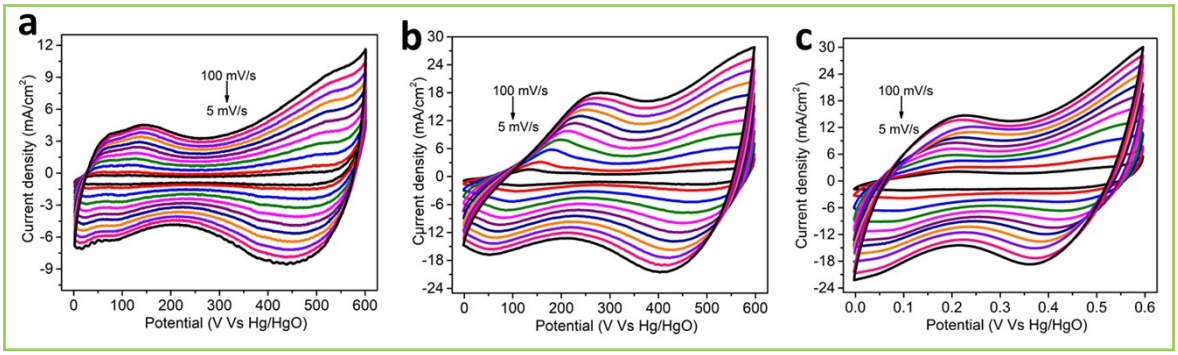

Figure S14 (a and b) CV curves of the $Co_3(PO_4)_2$/CC, CoPO-CMO21 and CoPO-CMO12 electrodes within scan rate range of 5 to 100 mV s^{-1}.

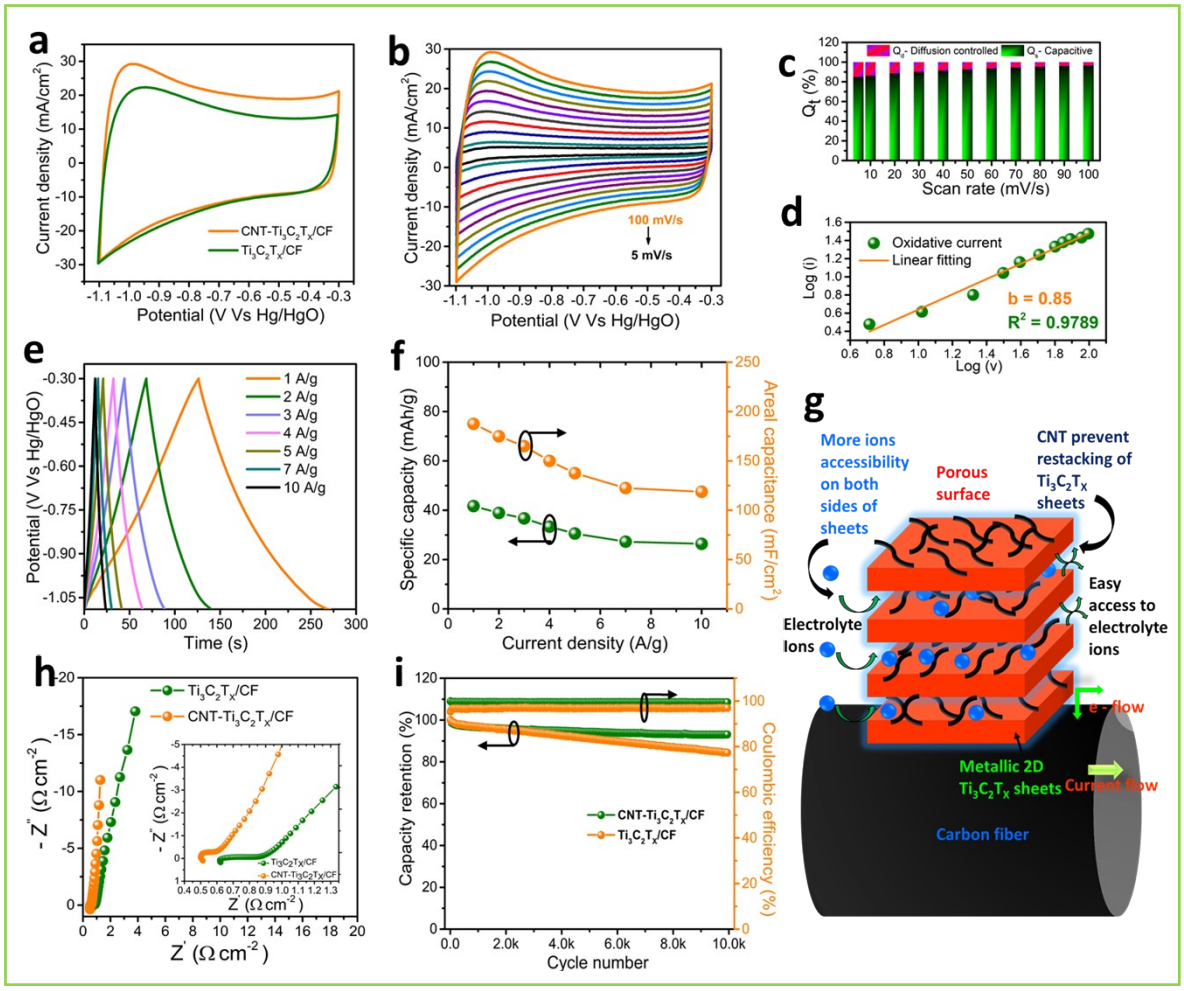

Figure S15 Electrochemical performance of CNT-$Ti_3C_2T_X$/CC electrode. (a) CV curve comparisons of $Ti_3C_2T_X$/CC and CNT-$Ti_3C_2T_X$/CC electrodes at 100 mV s^{-1} scan rate, (b) CV curves of a CNT-$Ti_3C_2T_X$/CC electrode at scan rates ranging from 5 to 100 mV s^{-1}, (c) the percent charge contribution from Q_s and Q_d sides, (d) a linear fitting plot of log current density (log(i)) vs log scan rate (log(v)) yields slope b and R^2 values, (e) GCD curves of CNT-$Ti_3C_2T_X$/CC electrode at different current densities of 1 – 10 A g^{-1}, (f) specific capacity and areal capacitance plots, (g) schematic diagram demonstrating the structural benefits of CNT-$Ti_3C_2T_X$/CC in terms of electrochemical reactivity (h and i) Nyquist plots and capacity retention and Coulombic efficiency vs cycle number plots of $Ti_3C_2T_X$/CC and CNT-$Ti_3C_2T_X$/CC electrodes.

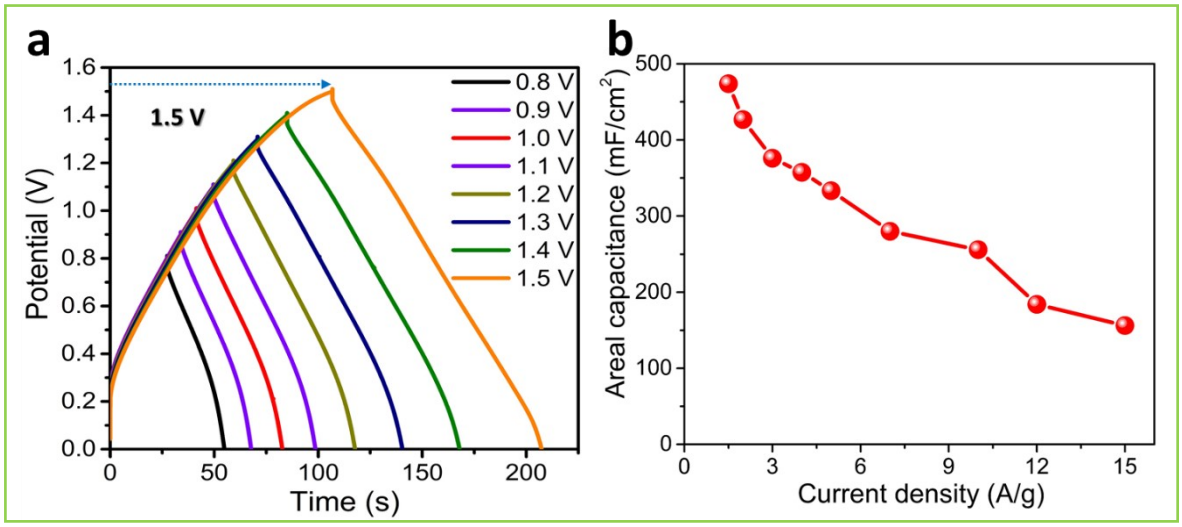

Figure S16 (a) Windows selection GCD curves and (b) Areal capacitance of CoPO-CMO238//CNT-$Ti_3C_2T_X$ FHSCs device at different current densities.

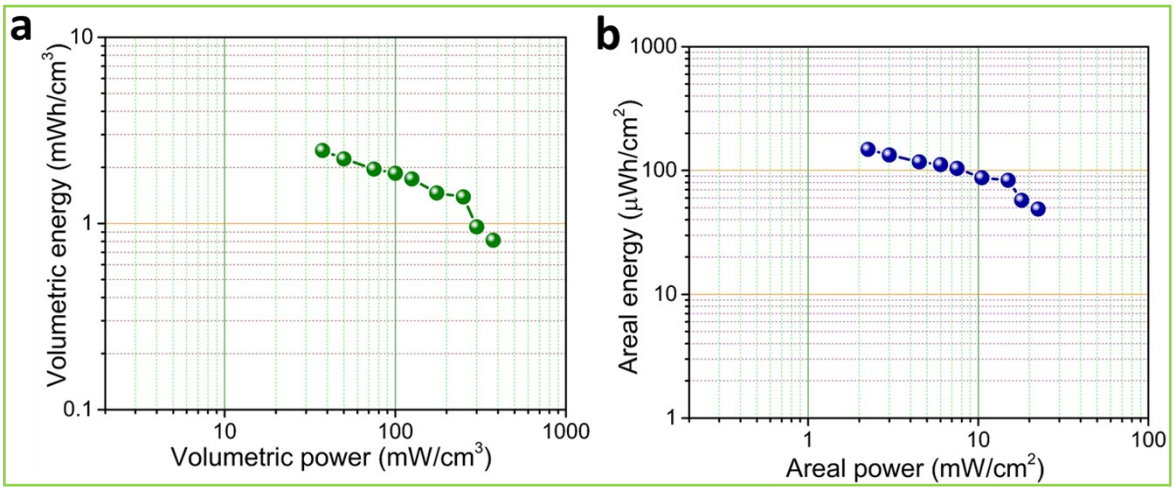

Figure S17 Volumetric and Areal energy and power (Ragone plots) of CoPO-CMO238//CNT-$Ti_3C_2T_X$ FHSCs device

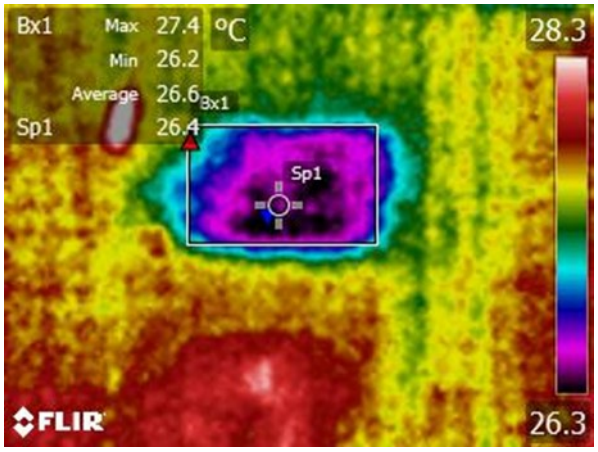

Figure S18 Temperature distribution image of FHSCs device.

Table S1 Comparison of electrochemical performance of phosphate-based electrodes with $Co_3(PO_4)_2/Co_2Mo_3O_8$ 2D-on-2D TSM/NS electrode.

Sr. No	Electrode Material	Method	Capacitance	Cycling Stability (%)	Ref.
1	$Co_3(PO_4)_2.8H_2O$/SS (Microplates/ Microflakes)	Hydrothermal	800 F g^{-1} at 2 mA cm^{-2}	83 % after 3000 cycles	[1]
2	$Co_3(PO_4)_2.4H_2O$ /GF	Hydrothermal	39.8 mAh g^{-1} at 10 A g^{-1}	-	[2]
3	$K_2Co_3(P_2O_7)_2 \cdot 2H_2O$ (Nanocrystal whiskers)	Hydrothermal	1100 mF cm^{-2} at 1.0 mA cm^{-2}	-	[3]
4	$Co_3(PO_4)_2$ (Leaf like, Nanoflakes)	Hydrothermal	410 F g^{-1} at 1 A g^{-1}	96.1 % after 2000 cycles	[4]
5	$NH_4CoPO_4.H_2O$ (Microbundles)	Hydrothermal	662 F g^{-1} at 1.5 A g^{-1}	92.7 % after 3000 cycles	[5]
6	$Co_3(PO_4)_2$ (Mesoporous)	Hydrothermal	247.7 F g^{-1} at 0.25 A g^{-1}	90 %	[6]
7	$NH_4CoPO_4.H_2O$ (Microflowers)	Chemical precipitation	525 F g^{-1} at 0.625 A g^{-1}	99.4% after 400 cycles	[7]
8	$NH_4CoPO_4.H_2O$ (Nano/Micro flowers/ plates)	Chemical precipitation	369.4 F g^{-1} at 0.625 A g^{-1}	99.7 % after 400 cycles	[8]
9	$Co_{11}(HPO_3)_8(OH)_6$ (Dumbbell like shape)	Hydrothermal	226 F g^{-1} at 1 A g^{-1}	76 % after 30 cycles	[9]
10	$Co_{11}(HPO_3)_8(OH)_6$ (Nano-ribbons)	Hydrothermal	312 F g^{-1} at 1.25 A g^{-1}	89.4 % after 3000 cycles	[10]
11	$Co_3(PO_4)_2$ (Nanoflakes)	Co-precipitation	188 F g^{-1} at 3 A g^{-1}	95 % after 80 cycles	[11]
12	$Co_3P_2O_8.8H_2O$ (Nanoparticles)	Chemical precipitation	446 F g^{-1} at 0.5 A g^{-1}	100 % after 3000 cycles	[12]
13	$Co_3P_2O_8.8H_2O$ (Flakes)	Chemical precipitation	205 F g^{-1} at 1 A g^{-1}	106 % after 100 cycles	[13]
14	$Co_3(PO_4)_2$ (Nanograss)	Hydrothermal	12,285 mF cm^{-2} at 5 mV s^{-1}	89 % after 600 cycles	[14]
15	$CoHPO_4.3H_2O$ (Layered)	Hydrothermal	413 F g^{-1} at 1.5 A g^{-1}	58.1 % after 300 cycles	[15]
16	$Co_3(PO_4)_2.8H_2O$ (Flower like)	Green precipitation	350 F g^{-1} at 1 A g^{-1}	102 % after 100 cycles	[16]
17	Ni-$Co_3(PO_4)_2 \cdot 8H_2O$	Chemical bath deposition	108 mAh g^{-1} at 0.5 A g^{-1}	78 % after 9000 cycles	[17]

18	$NH_4Co_3(HPO_4)_2(H_2PO_4)F_2$	Ionothermal	206.3 F g^{-1} at 1 A g^{-1}	80% after 300 cycles	[18]
19	$Co_{2.16}Mn_{0.84}(PO_4)_2$	Hydrothermal	571 F g^{-1} at a 2.2 A g^{-1}	88 % after 8000 cycles	[19]
20	$NH_4CoPO_4 \cdot H_2O$	Hydrothermal	158.5 mF cm^{-2} (43.3 F g^{-1}) 0.25 mA cm^{-2}	99 % after 3000 cycles	[20]
21	Cobalt phosphate/carbon (CoPi/C)	One-step carbonization	606.1 F g^{-1} at 1 A g^{-1}	94.2% after 000 cycles	[21]
22	$Co_3(PO_4)_2$/GF	Co-precipitation	21 mAh g^{-1}) at 0.5 A g^{-1}	89% after 5000 cycles	[22]
23	Cobalt hydrogen phosphate	hydrothermal	411.2 F g^{-1} at 1 A g^{-1}	97.6 % after 10000 cycles	[23]
24	$Co_2P_4O_{12}$	Solid-state sintering	437 F g^{-1} at 2.5 A g^{-1}	90 % after 3000 cycles	[24]
25	$Co_3(PO_4)_2@Co_2Mo_3O_8$	Hydrothermal/ Electrodeposition	184.7 mAh.g^{-1} at 1 A g^{-1}	95.6 % after 15000 cycles	**This Work**

Table S2 FHSCs device electrochemical performance comparison with previously reported supercapacitor devices.

Sr. No	Device	Capacitance	Specific energy	Specific power	Cycling Stability (%)	Ref.
1	$Co_3(PO_4)_2.4H_2O$/GF// C-FP	24 mAh g^{-1} at 10 A g^{-1}	24 Wh kg^{-1}	468 W kg^{-1}	99 % after 10000 cycles	[2]
2	$Co_3(PO_4)_2.8H_2O$//AC (Nanoflakes)	111.2 F g^{-1} at 5 mA cm^{-2}	5.33 Wh kg^{-1}	4687 W kg^{-1}	-	[25]
3	$Co_3P_2O_8.8H_2O$//AC (Nanoparticals)	55 F g^{-1} at 0.5 A g–1	11.9 Wh kg^{-1}	3.59 kW kg^{-1}	100 % after 3000 cycles	[12]
4	$Co_3P_2O_8.8H_2O$//AC (Flakes)	94 F g^{-1} at 0.5 A g–1	33.4 Wh kg^{-1}	399 W kg^{-1}	83 % after 5000 cycles	[13]
5	$Co_3(PO_4)_2$//AC (Nanograss)	85 F g^{-1} at 1 A g–1	26.66 Wh kg^{-1}	750 W kg^{-1}	80 % after 6000 cycles	[14]
6	$Ti_3C_2T_X$/Ag NP// MnO_2/ESCNF	246.2 mF cm^{-2}at 2 mA cm^{-2}	121.4 µW h cm^{-2}	17 395 µ W cm^{-2}	82 % after 10000 cycles	[26]
7	Co-MXene/PANIC@CFP	95.71 F g^{-1} at 1 A g–1	26.06 Wh kg^{-1}	700 W kg^{-1}	83 % after 8000 cycles	[27]
8	*m*-$WO_3/Ti_3C_2T_X$//MWCNT/RuO_2	145. F g^{-1} at 5 mV s^{-1}	27.2 Wh kg^{-1}	752 W kg^{-1}	93 % after 10000 cycles	[28]
9	β-$Ni(OH)_2$//MoS_2/MXene	153 F g^{-1}	54 Wh kg^{-1}	0.86 W kg^{-1}	90 % after 10000 cycles	[29]
10	MXene//V_2O_5	5.1 F g^{-1} at 10 A g^{-1}	8.33 mW h cm^{-3}	1053 mW cm^{-3}	61 % after 5000 cycles	[30]
11	$Ti_3C_2T_X$ - MXene//MnO_2	25 F g^{-1}	16.5 Wh kg^{-1}	160 W kg^{-1}	87 % after 8000 cycles	[31]
12	MXene//MnO_2	117.6 F g^{-1}	65.3 Wh kg^{-1}	2 k W kg^{-1}	93.58% after 6000 cycles	[32]

13	MXene/CoS 2//rGO	80.6 F g^{-1} at 1 A g^{-1}	28.8 Wh kg^{-1}	800 W kg^{-1}	98 % after 5000 cycles	[33]
14	Cx@rGO/$Ti_3C_2T_X$	64 F g^{-1} at 10 mV s^{-1}	~20 Wh kg^{-1}	480 W kg^{-1}	80 % after 10000 cycles	[34]
15	NiFe-LDH/MXene//AC	135.7 F g^{-1}	42.4 Wh kg^{-1}	758.27 W kg^{-1}	84 % after 1000 cycles	[35]
16	NiCo-MOF/$Ti_3C_2T_X$//AC	126.38 F g^{-1} at 1A g^{-1}	39.5 Wh kg^{-1}	562.5 W kg^{-1}	82.3 % after 10000 cycles	[36]
17	Co_2NiO_4/MXene ($Ti_3C_2T_X$)//AC	-	49.74 Wh kg^{-1}	752.21 W kg^{-1}	90.4 % after 3500 cycles	[37]
18	Ti_2CT_X@polyanilin e//Graphene	94.5 F g^{-1} at 1A g^{-1}	42.3 Wh kg^{-1}	950 W kg^{-1}	94.25% after 10000 cycles	[38]
19	MnO_2/ESCNF//Ti_3 C_2T_X/Ag	246.2 mF cm^{-2} at 2 mA cm^{-2}	121.4 μW h cm^{-2}	17 395 μW cm^{-2}	82 % after 10000 cycles	[26]
20	MXene-Ni-Co-LDH//MWCNT	-	36.70 Wh kg^{-1}	1.44 k W kg^{-1}	-	[39]
21	Ti_3C_2/Ni−Co−Al-LDH//AC	128.89 F g^{-1} at 0.5 A g^{-1}	45.8 Wh kg^{-1}	346 W kg^{-1}	97.8 % after 10000 cycles	[40]
22	$Co_3(PO_4)_2$@Co_2Mo $_3O_8$//CNT/$Ti_3C_2T_X$	7.9 F·cm^{-3} at 1.5 A g^{-1}	74.06 Wh kg^{-1}	1.13 kW kg^{-1}	93.2 % after 5000 cycles	**This work**

References

1. P. K. Katkar, S. J. Marje, S. S. Pujari, S. A. Khalate, A. C. Lokhande and U. M. Patil, *ACS Sustain. Chem. Eng.*, 2019, **7**, 11205-11218.
2. A. A. Mirghni, D. Momodu, K. O. Oyedotun, J. K. Dangbegnon and N. Manyala, *Electrochim Acta*, 2018, **283**, 374-384.
3. H. Pang, Y. Zhang, W.-Y. Lai, Z. Hu and W. Huang, *Nano Energy*, 2015, **15**, 303-312.
4. H. Mao, F. Zhang, X. Liu, J. Qiu, B. Li and Z. Jin, *J. Mater. Sci.: Mater. Electron.*, 2018, **29**, 16721-16729.
5. S. Wang, H. Pang, S. Zhao, W. Shao, N. Zhang, J. Zhang, J. Chen and S. Li, *RSC Adv.*, 2014, **4**, 340-347.
6. Y. Tang, Z. Liu, W. Guo, T. Chen, Y. Qiao, S. Mu, Y. Zhao and F. Gao, *Electrochim Acta*, 2016, **190**, 118-125.
7. Xinjun Wang, Zhenzhen Yan, Huan Pang, Weiqiang Wang, Guochang Li, Y. Ma, Hang Zhang, Xuexue Li and J. Chen, *Int. J. Electrochem. Sci*, 2013, **8**, 3768 - 3785.

8. H. Pang, Z. Yan, W. Wang, J. Chen, J. Zhang and H. Zheng, *Nanoscale*, 2012, **4**, 5946-5953.
9. D. H. Lee, M. Kang, S.-M. Paek and H. Jung, *Bull Korean Chem Soc*, 2016, **37**, 192-199.
10. H. Pang, Y. Liu, J. Li, Y. Ma, G. Li, Y. Ai, J. Chen, J. Zhang and H. Zheng, *Nanoscale*, 2013, **5**, 503-507.
11. J. Theerthagiri, K. Thiagarajan, B. Senthilkumar, Z. Khan, R. A. Senthil, P. Arunachalam, J. Madhavan and M. Ashokkumar, *ChemistrySelect*, 2017, **2**, 201-210.
12. J.-J. Li, M.-C. Liu, L.-B. Kong, M. Shi, W. Han and L. Kang, *Mater. Lett.*, 2015, **161**, 404-407.
13. M.-C. Liu, J.-J. Li, Y.-X. Hu, Q.-Q. Yang and L. Kang, *Electrochim Acta*, 2016, **201**, 142-150.
14. K. V. Sankar, S. C. Lee, Y. Seo, C. Ray, S. Liu, A. Kundu and S. C. Jun, *J. Power Sources*, 2018, **373**, 211-219.
15. H. Pang, S. Wang, W. Shao, S. Zhao, B. Yan, X. Li, S. Li, J. Chen and W. Du, *Nanoscale*, 2013, **5**, 5752-5757.
16. H. Li, H. Yu, J. Zhai, L. Sun, H. Yang and S. Xie, *Mater. Lett.*, 2015, **152**, 25-28.
17. B. N. Vamsi Krishna, S. Khaja Hussain and J. S. Yu, *J Colloid Interface Sci*, 2021, **592**, 145-155.
18. D. S. Pan, Z. H. Guo, J. K. Li, S. Huang, L. L. Zhou and J. L. Song, *Chemistry*, 2021, **27**, 7731-7737.
19. P. K. Katkar, S. J. Marje, V. G. Parale, C. D. Lokhande, J. L. Gunjakar, H. H. Park and U. M. Patil, *Langmuir*, 2021, **37**, 5260-5274.
20. L. Wannasen, E. Swatsitang and S. Pinitsoontorn, *Int. J. Energy Res.*, 2020, **45**, 3075-3088.
21. T. Kim, A. P. Tiwari, K. Chhetri, G. P. Ojha, H. Kim, S.-H. Chae, B. Dahal, B. M. Lee, T. Mukhiya and H. Y. Kim, *Nanoscale Advances*, 2020, **2**, 4918-4929.
22. B. A. Mahmoud, A. A. Mirghni, K. O. Oyedotun, D. Momodu, O. Fasakin and N. Manyala, *J. Alloys Compd.*, 2020, **818**.
23. Y. Wang, W. Li, L. Zhang, X. Zhang, B. Tan, J. Hao, Z. Jian, X. Wang, Q. Hu and X. Lu, *J. Power Sources*, 2020, **449**.
24. D. R. Patil, B. Koteswararao, K. Begari, A. Yogi, M. Moussa and D. P. Dubal, *ACS Appl. Energy Mater.*, 2019, **2**, 2972-2981.
25. H. Shao, N. Padmanathan, D. McNulty, O. D. C and K. M. Razeeb, *ACS Appl Mater Interfaces*, 2016, **8**, 28592-28598.
26. L. Li, N. Zhang, M. Zhang, L. Wu, X. Zhang and Z. Zhang, *ACS Sustain. Chem. Eng.*, 2018, **6**, 7442-7450.
27. Y. Zhang, J. Cao, Z. Yuan, L. Zhao, L. Wang and W. Han, *J Colloid Interface Sci*, 2021, **599**, 109-118.
28. A. M. Patil, J. Wang, S. Li, X. Hao, X. Du, Z. Wang, X. Hao, A. Abudula and G. Guan, *Chem. Eng. J*, 2021, **421**, 127883.
29. B. Kirubasankar, M. Narayanasamy, J. Yang, M. Han, W. Zhu, Y. Su, S. Angaiah and C. Yan, *Appl. Surf. Sci.*, 2020, **534**.
30. A. Qian, Y. Pang, G. Wang, Y. Hao, Y. Liu, H. Shi, C. H. Chung, Z. Du and F. Cheng, *ACS Appl Mater Interfaces*, 2020, **12**, 54791-54797.
31. Y. Zhu, K. Rajouâ, S. Le Vot, O. Fontaine, P. Simon and F. Favier, *Nano Energy*, 2020, **73**.
32. S. De, C. K. Maity, S. Sahoo and G. C. Nayak, *ACS Appl. Energy Mater.*, 2021, **4**, 3712-3723.
33. H. Liu, R. Hu, J. Qi, Y. Sui, Y. He, Q. Meng, F. Wei, Y. Ren, Y. Zhao and W. Wei, *Adv.*

Mater. Interfaces, 2020, **7**.
34. M. Boota, M. Rajesh and M. Bécuwe, *Mater. Today Energy*, 2020, **18**.
35. H. Zhou, F. Wu, L. Fang, J. Hu, H. Luo, T. Guan, B. Hu and M. Zhou, *Int. J. Hydrog. Energy*, 2020, **45**, 13080-13089.
36. Y. Wang, Y. Liu, C. Wang, H. Liu, J. Zhang, J. Lin, J. Fan, T. Ding, J. E. Ryu and Z. Guo, *Engineered Science*, 2020, DOI: 10.30919/es8d903.
37. J. Song, P. Hu, Y. Liu, W. Song and X. Wu, *ChemistrySelect*, 2019, **4**, 12886-12890.
38. J. Fu, J. Yun, S. Wu, L. Li, L. Yu and K. H. Kim, *ACS Appl Mater Interfaces*, 2018, **10**, 34212-34221.
39. H. Li, F. Musharavati, E. Zalenezhad, X. Chen, K. N. Hui and K. S. Hui, *Electrochim Acta*, 2018, **261**, 178-187.
40. R. Zhao, M. Wang, D. Zhao, H. Li, C. Wang and L. Yin, *ACS Energy Lett.*, 2017, **3**, 132-140.